Transportation Geotechnics 1 (2014) 188–200

Contents lists available at ScienceDirect

Transportation Geotechnics

journal homepage: www.elsevier.com/locate/trgeo

An integrated approach to dynamic analysis of railroad track transitions behavior

Debakanta Mishra [a,1], Yu Qian [a,2], Hai Huang [b,3], Erol Tutumluer [a,*]

[a] Department of Civil and Environmental Engineering, University of Illinois at Urbana-Champaign, 205 North Mathews Avenue, Urbana, IL 61801, United States
[b] Pennsylvania State University, Altoona, 3000 Ivyside Park, Altoona, PA 16601, United States

ARTICLE INFO

Article history:
Received 26 May 2014
Revised 1 July 2014
Accepted 1 July 2014
Available online 11 July 2014

Keywords:
Track dynamics
Instrumentation
Multidepth Deflectometers
Discrete Element Method
Analytical modeling
Ballast acceleration

ABSTRACT

Railway transitions like bridge approaches experience differential vertical movements due to variations in track stiffness, track damping characteristics, ballast settlement from fouling and/or degradation, as well as fill and subgrade settlement. Proper understanding of this phenomenon requires the integration of field instrumentation with analytical and numerical modeling. This paper introduces an integrated approach to dynamic analysis of the railway track transitions behavior using field instrumentation, analytical modeling, as well as numerical simulations using the Discrete Element Method (DEM). Several bridge approaches have been instrumented to monitor the track response on a problematic portion of the US North East Corridor (NEC), which is primarily a high-speed railway line with occasional freight traffic, carrying high-speed passenger trains operating up to a maximum speed of 241 km/h. Previous publications by the authors have focused on findings from geotechnical instrumentation of railroad track transitions, as well as the validity of a fully coupled 3-dimensional track dynamic model and image-aided discrete element models. The primary contribution of the current manuscript involves the combination of these three components to propose an integrated approach for studying the behavior of railroad track transitions. Track response data from instrumented bridge approaches were used to determine track substructure layer properties and calibrate a fully coupled 3-dimensional track dynamic model. Loading profiles generated from this model were then used as input for a discrete element based program to predict individual particle accelerations within the ballast layer. The importance of modeling the ballast layer as a particulate medium has been highlighted, and the particle to particle nature of load transfer within the ballast layer has been demonstrated.

Introduction

Railway track transitions present a significant challenge as far as maintenance of track profile is concerned. Due to the sudden change in track stiffness, the "stiff" side of a track transition undergoes lower deformations under loading, compared to the "less stiff" side. This differential movement often results in the formation of a "bump" in the track profile. Bridge approaches qualify as an ideal example of track transitions, with the approach track on either side of the bridge abutment being much less stiff compared to the bridge deck often supported by deep foundations. Differences in track system stiffness and/or damping characteristics, settlement of the ballast layer due to degradation and/or fouling, and settlement of the subgrade and/or fill

* Corresponding author. Tel.: +1 217 333 8637.
E-mail addresses: dmishra2@illinois.edu (D. Mishra), yuqian1@illinois.edu (Y. Qian), huh16@psu.edu (H. Huang), tutumlue@illinois.edu (E. Tutumluer).
[1] Tel.: +1 217 244 2587.
[2] Tel.: +1 217 799 4558.
[3] Tel.: +1 814 949 5346.

http://dx.doi.org/10.1016/j.trgeo.2014.07.001
2214-3912/

layers are some of the factors commonly reported as mechanisms contributing to the differential movement at track transitions. Proper understanding of different mechanisms contributing to this phenomenon requires the combined application of field instrumentation with analytical and numerical track modeling. Several research studies have focused on investigating the bump development at both highway and railway bridge approaches (Zaman et al., 1991; Stark et al., 1995; Briaud et al., 1997; White et al., 2005; Briaud et al., 2006; Nicks, 2009). A detailed review of these past research efforts, different factors contributing to the bump development at railway track transitions, as well as the effects of possible remedial measures has been presented by Mishra et al. (2012).

Due to the sudden change in track profile, railway track transitions are often exposed to magnified dynamic loads as a train passes over them. Such magnified load levels ultimately result in rapid degradation in track geometry and profile, requiring frequent maintenance and resurfacing. The annual expenditure to maintain track transitions in the US has been reported to exceed USD 200 million (Sasaoka et al., 2005; Hyslip et al., 2009). Nicks (2009) reported that approximately 50% of railroad bridge approaches in North America experienced differential movement problems, characterized by the development of a low approach, usually 6–102 mm in depth. Read and Li (2006) reported that the bump problem is more significant at the "exit" side of a transition, as the train moves from a high-stiffness track to a low-stiffness track. The "bump" formation at railway bridge approaches is usually within 15 m from the abutment (Plotkin and Davis, 2008).

The differential movement at track transitions is particularly problematic for high-speed rail infrastructure as the "bump" is accentuated at high speeds. The issue is even more critical for shared corridors carrying both freight and high-speed passenger trains. Transitions along shared corridors need to be maintained to satisfy the high ride quality requirements associated with high-speed trains. Additionally, these transitions also need to withstand the heavy loads imposed by slow-moving freight trains without undergoing excessive deformations. With the current impetus for development of high speed lines in the US and the challenges associated with shared corridors for operation of passenger trains at increased speeds, preventing and mitigating the problem of differential movement at bridge approaches and other track transitions has become more significant.

This paper introduces an integrated approach to dynamic modeling of railway track transitions through field instrumentation and analytical and numerical modeling. Field instrumentation data collected from Multidepth Deflectometers (MDDs) and strain gauges are used to determine individual track substructure layer deformations and dynamic wheel loads, respectively. Track response data from instrumented bridge approaches are then used to calibrate a fully coupled 3-dimensional dynamic track model. Loading profiles generated from this model are used as input for a numerical simulation program based on the Discrete Element Method (DEM) to predict individual particle accelerations within the ballast layer. Shortcomings associated with other track analysis and numerical modeling approaches based on the principles of finite element, or finite difference methods to characterize the ballast layer as one continuum are highlighted. Accordingly, through the integrated approach, the importance of modeling the ballast layer as a particulate medium is mainly emphasized, and the particle to particle contact for load transfer within the ballast layer is demonstrated. Therefore, the primary objective of this paper is to emphasize the importance of adopting an integrated approach for realistic analyses of ballasted railroad track systems. This has been accomplished with the help of instrumentation and numerical modeling results from different track transition sections. Proposing solutions to mitigate the differential movement problem at track transitions is beyond the scope of this paper.

Field instrumentation of selected track transitions

A research study sponsored by the US Federal Railroad Administration (FRA) is currently being carried out at the University of Illinois with the overall objective of identifying and mitigating different factors contributing to the differential movement at railway transitions. Several problematic track transitions have been instrumented under the scope of the current study to monitor the track response under loading near Chester, Pennsylvania on Amtrak's North East Corridor (NEC). There are 8–10 closely-spaced undergrade bridges with recurring differential movement problems at the bridge/embankment interfaces. The NEC is primarily a high-speed railway with occasional freight traffic, carrying high-speed passenger trains operating up to a maximum speed of 241 km/h. This segment of the NEC near Chester comprises four tracks, with Tracks 2 and 3 maintained for high-speed Acela Express passenger trains operating at 177 km/h. The predominant direction of traffic along Track 2 is Northbound whereas Track 3 primarily carries Southbound traffic. Data from the instrumented track transitions are being used to calibrate different analytical and numerical models to predict the dynamic track behavior under train loading. A brief description of the instrumentation used in the current study is first presented in the sections below.

Instrumentation details

The instrumentation used in the current study comprised Multidepth Deflectometers (MDDs) for measuring track substructure layer deformations, and strain gauges mounted on the rail for measuring the vertical wheel loads and tie support reactions. The MDD technology was first developed in South Africa in the early 1980s to measure individual layer deformations in highway pavements (Scullion et al., 1989). MDDs typically consist of up to six linear variable differential transformers (LVDTs) installed vertically at preselected depths in a small diameter (45 mm in the current study) hole to measure the deformation of individual track layers with respect to a fixed anchor buried deep in the ground (DeBeer et al., 1989). More details on the operation principle of MDDs can be found elsewhere (Mishra et al., 2012; DeBeer et al., 1989). It is noteworthy

that the use of MDDs to monitor railway track performance has been extensively pursued in South Africa (Gräbe and Clayton, 2005; Gräbe and Shaw, 2010; Priest et al., 2010; Vorster and Gräbe, 2013). Any boundary effects and associated stress concentrations introduced in the track substructure layers due to drilling of the MDD hole (hole diameter is 45 mm; mean particle size or D_{50} of ballast is approximately 35 mm) are assumed to be of negligible significance, and therefore have not been considered during analyses of the instrumentation data.

Fig. 1 shows the schematic of an MDD system with five LVDT modules each installed at track substructure layer interfaces. Individual LVDTs are placed at different depths inside the borehole to measure the deflections at (1) top of ballast layer, (2) top of fouled ballast layer, (3) top of embankment fill layer 1, (4) top of embankment fill layer 2, and (5) top of the subgrade layer, respectively. The approach fill layer or the subgrade as indicated in Fig. 1 can conceptually be divided into two separate segments: "deformable" and "non-deformable," respectively. The MDD anchor is fixed at a depth that is assumed to be in a "non-deformable" subgrade or approach fill. Note that the deformations of substructure layers measured using the MDD technology is dependent on the assumption that the anchor is located in a non-deformable layer, and does not undergo any elastic or permanent deformation. Accordingly, for an accurate measurement of layer deformations using MDDs installed on a bridge approach, it is important to ensure that the anchor is located sufficiently below the track level. Track construction reports and/or reports from previous geotechnical explorations (if available) can be used to make educated inferences regarding the potentials of individual track substructure layers to accumulate transient (elastic) and permanent (plastic) deformations under loading. This information can also be used to identify suitable locations for placement of the MDD anchor.

The MDD system involves the installation of a flexible lining tube in the drilled hole; individual LVDT modules are subsequently mounted inside the hole by gripping against the flexible lining tube. Additionally, a polyurethane grout is used to ensure proper contact between the flexible lining tube and the adjacent soil layers. Presence of the polyurethane grout and the flexible lining tube provides sufficient flexibility to the LVDT mounting points to ensure adequate insulation against vibrations transmitted from the upper layers. Moreover, no physical connection exists between individual LVDT modules in an MDD system. Accordingly, transmission of vibrations from the upper layers can be adequately avoided.

Note that due to the presence of overhead catenary cables, the boreholes for MDD installation in the current study could not be drilled deeper than 3.0 m below the top of the tie. Accordingly, the MDD anchor was placed at a depth of 3.0 m below the top of the crosstie. However, this is likely to be sufficient to ensure the "non-deformability" of the anchor, as the instrumented sites have been in service for more than 100 years. Accordingly, the embankment fill and subgrade layers have likely been fully consolidated, resulting in no significant elastic or plastic deformations.

Track substructure layer configuration

The track substructure layer profile was determined during the drilling by visual classification of the soil coming out of the drilled hole. The drilling was carried out in small (25–50 mm) increments to ensure that the depths of substructure layer interfaces could be identified with reasonable accuracy. The positions of individual MDD modules correspond to changes in the track substructure layer interfaces as determined during the drilling process. Fig. 2 shows the layer profile established during the instrumentation of one of the bridge approaches. Note that the term "fouled ballast" has been used to indicate the section of ballast layer that was contaminated with fine materials from underlying layers. Accordingly, this terminology is not intended to make references to the quality of ballast material used in the instrumented approaches.

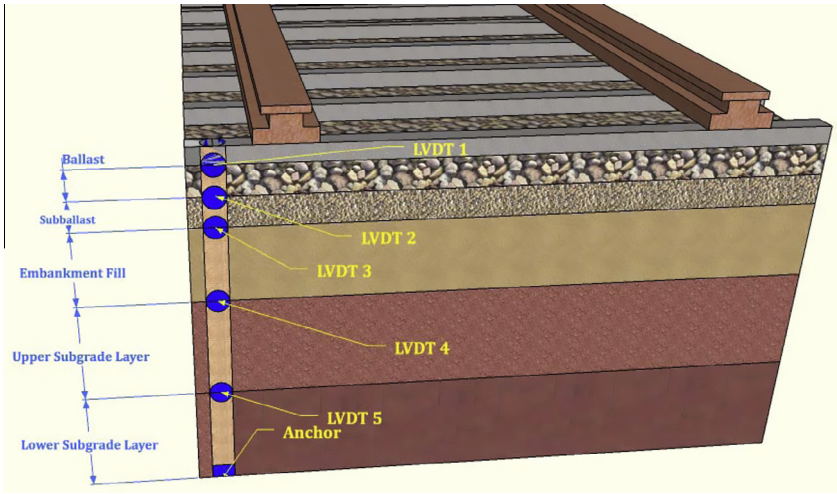

Fig. 1. Schematic representation of multidepth deflectometer (MDD) system installed in railroad track.

It is important to highlight that the extent of fouling in the ballast layer is a transient phenomenon, and hence the position of the ballast-fouled ballast layer interface is likely to shift over time. For the purpose of this study, the position of this interface has been assumed to be stationary at the position identified during the drilling process. Subsequently, the ballast and fouled ballast layers have been treated as two separate layers for analytical and numerical modeling purposes, and different layer moduli have been assigned to the two layers. Characterization of the ballast-fouled ballast layer interface transient behavior requires extensive investigations through periodic subsurface explorations potentially utilizing ground penetrating radar (GPR) scanning and is beyond the scope of the current paper.

In addition to the MDDs, strain gauges were also installed on the rail to measure the vertical wheel load and tie reaction forces. A total of eight (8) strain gauges (two sets of four, constituting two different Wheatstone bridges) were installed next to each MDD hole.

Periodic monitoring and data acquisition

Two types of data are currently being collected from the instrumented bridge approaches to monitor and evaluate their performances. To monitor the permanent deformation accumulations in individual track substructure layers, "offset measurements" are being collected from the instruments at one to two week intervals. Additionally, transient (recoverable) deformations are also being collected for each approach under train loading at two to three month intervals. Periodic data acquisition was carried out using a laptop computer and a signal conditioner connected to the installed sensors. All LVDTs used in the MDD system were manufactured using an inductive half-loop configuration, and were excited using an AC power of 1 V at 4.8 kHz. The strain gauge circuits were powered by an excitation of 5 V magnitude. The data acquisition frequency for monitoring the transient track response under train loading was 2000 Hz. Fig. 3 presents the transient data collected from one of the instrumented bridge approaches during the passage of an Amtrak Acela Express passenger train. Note that both transient and permanent track deformations recorded in this study have been analyzed in view of the contributions of individual layers only. In other words, only the percentages of total track deformations contributed by individual layers have been determined. Analyses of individual mechanisms contributing to the individual layer deformations are beyond the scope of the current paper. Accordingly, different mechanisms such as ballast degradation, ballast migration, particle rearrangement, that can contribute significantly towards deformations within the ballast layer have not been separately investigated.

A typical ACELA Express train comprises two power cars (one at either end) separated by six passenger cars. This configuration of the train is clearly reflected by the vertical wheel load values registered by the strain gauges installed on the rail (see Fig. 3-a). The heavier power cars apply higher loads on the rail compared to the passenger cars. Moreover, the peaks corresponding to individual axles (32 in total) passing over the instrumentation location is clearly evident from the graph. Fig. 3-b shows the transient deformations recorded by the top LVDT under the passage

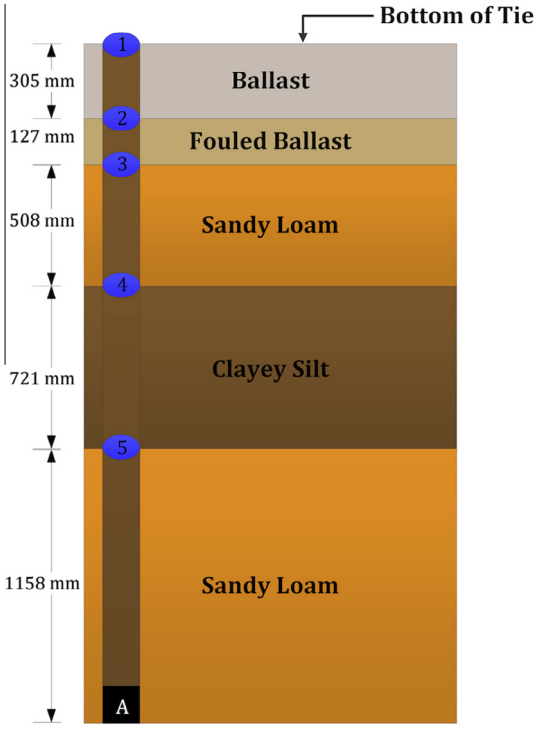

Fig. 2. Substructure layer profile for instrumented track section analyzed (the numbers 1 through 5 indicate the positions of the LVDTs installed along the hole for measuring individual substructure layer deformations).

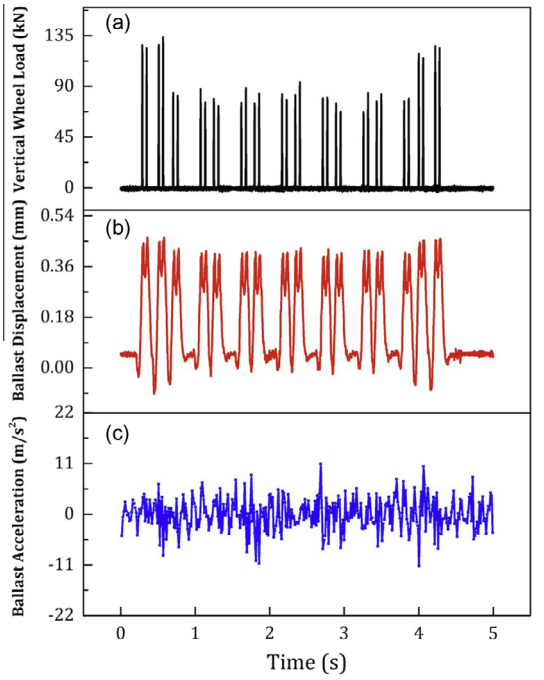

Fig. 3. Field measured values for (a) vertical wheel load applied on top of rail, (b) ballast layer deflection, and (c) ballast layer acceleration.

of the same train. Note that the top LVDT was mounted within the concrete crosstie, just above the top of the ballast layer. As the concrete crosstie is rigid, and does not undergo any deformation under loading, the deformations recorded by the top LVDT can be assumed to represent the deformation within the ballast layer. However, it is important to note that the deformations registered by the top LVDT may include excessive deformations of the crosstie resulting from inadequate support conditions underneath, also referred to as "hanging tie" conditions. Fig. 3-c shows the layer acceleration values calculated for the ballast layer from the LVDT-recorded transient deformations.

Estimation of track substructure layer moduli using GEOTRACK

The transient data collected under train passage from the instrumented bridge approaches were used to iteratively estimate the track substructure layer moduli. A three-dimensional, multi-layer elastic model GEOTRACK was used for this purpose. The GEOTRACK program was initially developed by Chang et al. Chang et al. (1980), and has been validated by previous studies (Stewart and Selig, 1982a,b) to closely match the elastic response of railroad tracks in operation. The basic assumptions and features of GEOTRACK program are listed in Table 1.

Peak transient displacements corresponding to the last two wheels on the trailing locomotive were used for estimating the substructure layer modulus values. The corresponding wheel loads measured by the strain gauge circuits were used as input in the GEOTRACK software. Note that the strain gauge circuits installed under the scope of this study were based on the principle of measuring the shear strains induced at the neutral axis of the rail, and accordingly, did not distinguish between dynamic and static components of the loads applied to the rail. Therefore, the load levels recorded by strain gauges during the current study include the dynamic components imposed due to track/wheel irregularities. These load levels were used as "static" inputs for the GEOTRACK analyses. Peak transient deformations recorded by the individual LVDTs corresponding to the time, when the leading wheel of the trailing locomotive was directly on top of the instrumented tie, were used as the substructure layer deformations. Position of the second wheel load was determined based on the axle spacing (obtained from the locomotive manufacturers) and tie spacing patterns at the instrumented bridge approaches. For instances where the second wheel location was between two ties, standard force and moment balance methods were used to assign representative vertical load values to individual ties. An example set of measured transient deformations corresponding to the layer profile shown in Fig. 2 is presented in Table 2. Typical track parameters used during the GEOTRACK analyses are listed in Table 3.

The moduli of individual substructure layers were changed iteratively to match the GEOTRACK-predicted deformations at the substructure layer interfaces with those recorded in the field. Special care was adopted to account for the underlying assumption in the MDD measurement system regarding the "non-deformability of the anchor". Accordingly, the GEOTRACK-predicted elastic deformation at a depth corresponding to the anchor position was subtracted from the predicted deformations at each substructure layer interface. This procedure was repeated until an exact match was obtained between the GEOTRACK-predicted and field-measured elastic deformation values corresponding to the MDD module positions. Fig. 4 presents an example case showing the exact match between field-measured and GEOTRACK-predicted deformations at different depths within the track substructure obtained through iterative adjustment of layer moduli. The following moduli values in MPa, from top to bottom, were obtained from this iterative estimation scheme for the substructure layer profile presented in Fig. 2: 69, 55, 31.5, 32, and 69, respectively. These modulus values were subsequently used as input into the fully coupled 3-dimensional analytical track model explained below. Note that the layer moduli listed above were not directly measured in the field. Rather, the GEOTRACK-predicted layer deformations were iteratively matched with the transient deformations measured using the MDDs by adjusting the individual layer moduli.

It is important to note that the data analysis in the current manuscript focuses on transient response of the track only. Accordingly, the substructure layer moduli calculated in this section correspond to instantaneous transient response of the track under train loading. Accordingly, no consideration has been given to the effects of repeated loading or cumulative damage on track behavior.

Table 1
Inherent Features and Assumptions of the GEOTRACK Program

General	• 3-Dimensional multilayer • Up to 5 substructure layers • Infinite horizontal extent • No slip at layer interfaces • Only vertical loading considered
Rail	• Linear elastic beams • Spans eleven ties • Free to rotate at ends, and at each tie • Linear spring connection between rail and tie
Ties	• Linear elastic beams • Supported at 10-equally spaced circular locations by the underlying ballast

A fully coupled 3-dimensional model for dynamic analysis of tracks

The integrated approach introduced in this paper presents the combined application of field-instrumentation

Table 2
Typical transient deformation values recorded by MDDs at track substructure layer interfaces.

Layer interface depth (mm)	Cumulative deflection (mm)
0	1.716
304.8	1.253
431.8	1.009
939.8	0.567
1661.16	0.183
2514.6	0

Table 3
Typical track parameters used during GEOTRACK analyses.

Track variable	Value used
(1) Rail properties	
Spacing (mm)	1510
Cross area (mm^2)	8650
E (MPa)	2.07E + 05
Weight (kg/m)	66.81
I (mm^4)	3.95E + 07
Fastener or tie pad stiffness (kN/m)	1.20E + 06
(2) Tie properties	
Length (mm)	2591
Center to center tie spacing (mm)	610
Tie width at base of tie (mm)	274
Tie width (mm)	228.6
Tie height (mm)	177.8
E (MPa)	2.07E + 04
Tie weight (kg)	386
No. of tie segments having centers between the rails	6
I (mm^4)	2.42E + 08
(3) Material properties	
Unit weight (kN/m^3; layers from top to bottom)	19.5, 20.5, 20.5, 20.5, 20.5
Poisson's ratio (layers from top to bottom)	0.3, 0.4, 0.4, 0.4, 0.4
(4) Wheel load	
Tie number	1, 5, 6
Magnitude (tonnes)	*12.6, 5.045, 7.355*

along with analytical and numerical track modeling. Wheel load and transient layer deformation values collected from the instrumented bridge approaches under train loading were first used to calibrate a fully coupled three dimensional train-track-soil model developed by Huang et al. (2014). This model is a modified version of the 3-D Sandwich model developed by Huang et al. (2010), and characterizes the subgrade as a three-dimensional plane stress finite element mesh. Additionally, the rail is modeled as an Euler beam discretely supported at points corresponding to the tie locations. Each rail pad, tie, and ballast system is modeled using a combination of mass, spring, and damper. The train is modeled as a simplified Type I vehicle with both primary and secondary suspensions having 10 degrees of freedom. The governing equations for the fully coupled 3-D track model, described in detail by Huang et al. (2010), are presented in the following subsections.

Analytical representation of train loading

The governing equation for the train loading can be expressed as:

$$[K - \omega^2 M]\{dV(w)\} = \{f(w)\} \tag{1}$$

where "K" and "M" are the stiffness matrix and mass (including mass moment of inertial) matrices of the car, respectively. "$\{dV(\omega)\}$" is the nodal displacement vector. "$f(\omega)$" is the nodal external force vector. Since $\{f(\omega)\} = \begin{bmatrix} 0 \\ I \end{bmatrix}\{P(\omega)\}$ where "$\{P(\omega)\}$" is the nodal wheel force vector and $\{dW(\omega)\} = [0 \quad I]\ \{dV(\omega)\}$, Eq. (1) can be rewritten as:

$$\{dW(\omega)\} = [GV]\{P(\omega)\} \tag{2}$$

where $[GV] = [0 \quad I][K - \omega^2 M]^{-1}[0 \quad I]^T$ is called "Green Function of the Vehicle." Note that Eq. (2) is the relationship between the wheel displacement and the wheel rail contact forces in the frequency domain. By applying forces $\{P\}$ on the wheels at a frequency "ω", those wheels will vibrate with magnitudes of "dW".

Analytical representation of discrete tie support

The discrete nature of tie support can be analytically modeled by the following set of equations, as explained in detail by Huang and Brennecke (2013).

$$a_m(t) = (U_r(x_m, t) - U_t(x_m, t))K_p(m) + \left(\dot{U}_r(x_m, t) - \dot{U}_t(x_m, t)\right)D_p(m) \tag{3}$$

$$b_m(t) = (U_b(x_m, t) - U_a(x_m, t))K_b(m) + \left(\dot{U}_b(x_m, t) - \dot{U}_a(x_m, t)\right)D_b(m) \tag{4}$$

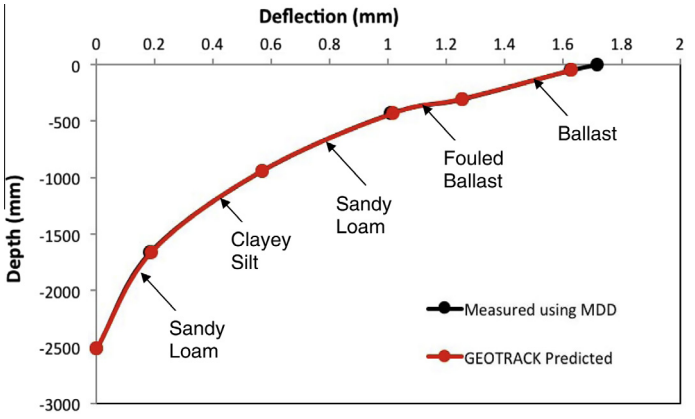

Fig. 4. Matching the field measured and GEOTRACK predicted deflections at different positions within the track substructure through iterative estimation of substructure layer moduli.

$$(U_r(x_m,t)-U_t(x_m,t))K_p(m)+\left(\dot{U}_r(x_m,t)-\dot{U}_t(x_m,t)\right)D_p(m)-(U_t(x_m,t)-U_b(x_m,t))K_b(m)+\left(\dot{U}_t(x_m,t)-\dot{U}_b(x_m,t)\right)D_b(m)=M_t(m)\ddot{U}_t(x_m,t) \quad (5)$$

$$(U_t(x_m,t)-U_b(x_m,t))K_b(m)+\left(\dot{U}_t(x_m,t)-\dot{U}_b(x_m,t)\right)D_b(m)-(U_b(x_m,t)-U_a(x_m,t))K_b(m)+\left(\dot{U}_b(x_m,t)-\dot{U}_a(x_m,t)\right)D_b(m)=M_b(m)\ddot{U}_b(x_m,t) \quad (6)$$

where

$a_m(t)$ = compression force at mth tie between rail and support as a function of time;
$b_m(t)$ = compression force at the mth tie between support and soil as a function of time;
$U_r(x_m, t)$ = rail deflection at mth tie as a function of time;
$U_t(x_m, t)$ = tie deflection at mth tie as a function of time;
$U_b(x_m, t)$ = ballast top vertical displacement at mth tie as a function of time;
$U_a(x_m, t)$ = soil surface deflection at mth tie as a function of time;
$K_p(m)$ = stiffness of mth pad;
$D_p(m)$ = damping of mth pad;
$K_b(m)$ = stiffness of ballast at mth tie position;
$D_b(m)$ = damping of ballast at mth tie position;
$M_t(m)$ = mass of mth tie; and
$M_b(m)$ = equivalent mass of ballast under the mth tie.

Analytical representation of rail

The rail is modeled as an Euler Bernoulli beam, and can be represented by the following equation:

$$EIU_r(x,t)'''' + \rho U_r(\ddot{x},t)+\varepsilon U_r(\dot{x}t)+TU_r(x,t)'' = f(t)\delta(x-vt)-\sum_m a_m(t)\delta(x-x_m) \quad (7)$$

where

EI = bending stiffness of rail;
$U_r(x, t)$ = rail deflection as a function of time;
ρ = Unit mass of rail;
ε = damping of rail (set to zero for convenience);
T = rail axial force caused by temperature increase;
$f(t)$ = wheel load function;
δ = Dirac delta function;
x_m = location of the mth tie; and
v = wheel speed.

Analytical representation of 3-dimenstional soil support

The subgrade underneath the ballast layer is represented using a 3-dimensional finite element model. The following conceptual equation can be used for representing the 3-D soil layer:

$$\{U_a(x_m,\omega)\}=[GS]\times\{b_m(\omega)\} \quad (8)$$

where ω represents the frequency, and $[GS]$ is Green's function of the soil and can be solved by the following equation:

$$([K_s]-(\omega-\lambda v)^2\times[M])\times\left[\overline{dS}\right]=[\overline{F}] \quad (9)$$

where

$[K_s]$ = stiffness matrix of the soil;
λ = wave number;
v = train speed;
$\overline{dS}$ = soil displacement vector; and
$[\overline{F}]$ = force acting on top of the soil.

Analytical representation of train-track-soil coupling

The contact between the wheel and the track was modeled using a Hertzian contact spring with Stiffness = HK. The mathematical representation of the wheel–rail contact is illustrated below:

$$-\{dW(\omega)\}-\{dR(\omega)\}-\{ds(\omega)\}=\frac{\{P(\omega)\}}{[HK]} \quad (10)$$

where

$\{dR(\omega)\}$ is the downward rail displacement in the frequency domain;
and $\{ds(\omega)\}$ is the combination of rail surface roughness and train speed, which induces vibrations in the vehicle (obtained through field measurements).

The overall track deflection and wheel-rail contact forces can be represented by the equation:

$$\{dR(\omega)\}=[GT]\{P(\omega)\} \quad (11)$$

where $[GT]$ is the Green Function of the track, accordingly, the wheel-rail contact force can be expressed by using the rail surface roughness and train speed:

$$\{P(\omega)\}=-([HK][GV]+[HK][GT]+[I])^{-1}\{ds(\omega)\} \quad (12)$$

Validation and verification of results obtained from the fully coupled 3D analytical track model have been presented in previous publications by Huang et al. Huang et al. (2014), Huang and Brennecke (2013), Huang et al. (2009). Fig. 5 shows a schematic representation of the dynamic track model used in the current study.

The track substructure profile presented in Fig. 2 was used in the dynamic track modeling approach to model all the layers underlying the ballast layer. Accordingly, the modulus values for these layers were adjusted until the layer deformations predicted by the analytical model closely corresponded to those measured in the field. This final combination of layer modulus values was then used to determine the load levels transmitted to the ballast layer. Fig. 6 shows the load levels applied on top of the ballast layer, as predicted by the analytical track model. As expected, the load levels on top of the ballast are significantly lower than those measured on the rail using strain gauges. Moreover, the analytical track model also predicts higher load levels corresponding to the power car compared to the passenger cars. The maximum load level applied on the ballast layer is 23.3 kN, which is 17% of the maximum load value measured on the rail (134 kN). Note that the load levels on top of the ballast layer presented in Fig. 6 are obtained from the analytical model results only. This is because the field instrumentation effort did not involve the measurement of load levels on

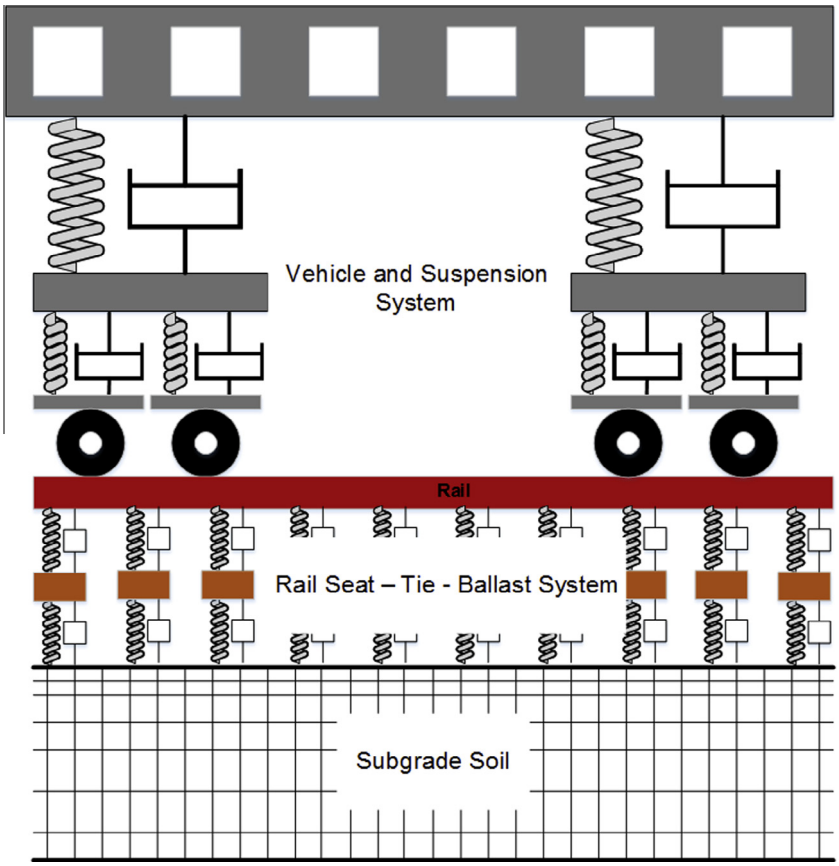

Fig. 5. Schematic representation of fully-coupled 3D track model by Huang et al. (2014).

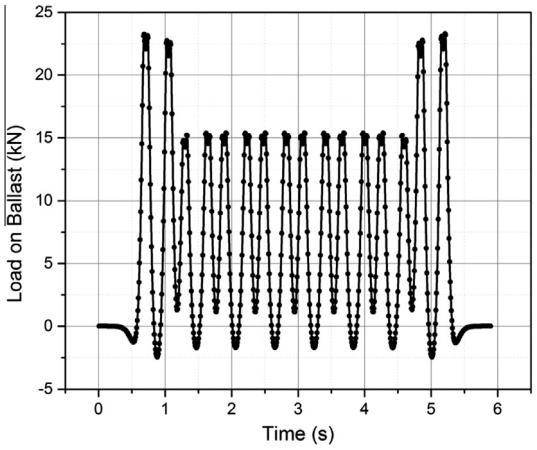

Fig. 6. Load levels applied on the ballast layer as predicted by the fully coupled 3-dimensional dynamic track model.

the ballast layer (load levels were measured through strain gauges installed on the rail only). It is important to note that additional instrumentation to measure the load levels on top of the crosstie as well as on top of the ballast layer will no doubt aid validation of the analytical and numerical models. However, such measurements are beyond the scope of the current research study.

Image-aided discrete element modeling of ballast layer

The load levels predicted by the dynamic track model on top of the ballast layer were used as inputs to an image-aided DEM program to predict the ballast layer behavior. This image-aided DEM simulation approach developed at the University of Illinois has the capability to create actual ballast aggregate particles as three-dimensional polyhedron elements having the same particle size distributions and imaging quantified average shapes and angularities. Ghaboussi and Barbosa (1990) developed the first polyhedral 3D DEM code BLOCKS3D for particle flow; and Nezami et al. (2006) enhanced the program with new, fast contact detection algorithms. Tutumluer et al. (2006) combined the DEM program and the aggregate image analysis together to simulate the ballast behavior more accurately and realistically by using polyhedral elements regenerated from the image analysis results of ballast materials. This DEM approach was first calibrated by laboratory large-scale direct shear test results for ballast size aggregate application (Huang and Tutumluer, 2011). The calibrated DEM model was then utilized to model strength and settlement behavior of railroad ballast for the effects of multi-scale aggregate

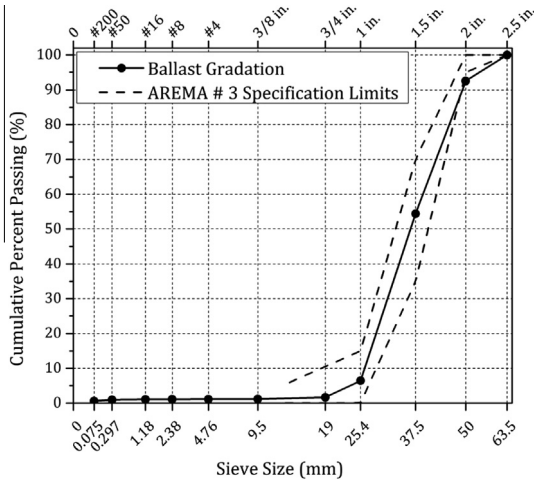

Fig. 7. Particle size distribution of ballast material used on site.

morphological properties (Tutumluer et al., 2006, 2007). A successful field validation study was also conducted with the ballast DEM simulation approach through constructing and monitoring field settlement records of four different ballast test sections and then comparing the measured ballast settlements under monitored train loadings to DEM model predictions (Tutumluer et al., 2011).

The first step to use the image-aided DEM modeling approach in this study involved collecting representative ballast materials from the instrumented bridge approaches. The typical particle size distribution of the ballast material was first established in the laboratory through sieving, as shown in Fig. 7. The ballast material corresponded to US AREMA # 3 gradation. Besides sieving, ballast particles corresponding to different sieve sizes were also scanned using the University of Illinois Aggregate Image Analyzer (UIAIA) to establish imaging-based particle morphological indices such as the Angularity Index (Rao et al., 2002), Flat and Elongated Ratio (Rao et al., 2001), and Surface Texture Index (Rao et al., 2003). The average values for these imaging based morphological indices were found to be 384, 2.2, and 1.4, respectively. Fig. 8 illustrates the steps involved in creating 3-dimensional polyhedron elements corresponding to individual ballast particles to be used in discrete element modeling of railroad track structures.

These morphological indices were subsequently used to select representative polyhedral ballast particles to constitute the track model using a discrete element program (BLOKS3D) developed at the University of Illinois. Fig. 9 shows the dimensions of the half-track model generated using the BLOKS3D program, used in this study.

Different steps followed to create the half-track model using the BLOKS3D program are listed below: (1) create a particle library to match the aggregate morphological properties established through image analysis; (2) drop the particles to form a cuboid section; (3) compaction stage I: use one top platen to compact the ballast particles by pressing downwards; all the side and bottom boundaries simulated as rigid during this stage; (4) release the rigid boundary on the left hand side of the model to form the ballast shoulder slope; (5) compaction stage II: use one top platen and one side platen (on a 2:1 slope) to compact the section without changing its shape; (6) delete the compaction platens and extra particles from the model; (7) set the tie and rail on top of the compacted ballast layer at the appropriate location; (8) modify the boundary properties to have the same contact stiffness as the ballast to ballast particle contact; (9) apply the load history determined from the analytical track model.

It is important to note that the boundary immediately underneath the ballast layer was also assigned a stiffness value equal to the inter-particle contact stiffness. Accordingly, the boundary underneath the ballast layer was assumed to be rigid and non-deformable, and therefore, the primary area of interest for the DEM modeling approach is the individual particle behavior within the ballast layer. The acceleration time histories for individual ballast particles at different positions along within the ballast layers were monitored, and inferences regarding the layer behavior were drawn.

Results and discussion

Fig. 10 presents individual ballast particle acceleration levels determined at different positions within the ballast layer using the BLOKS3D program. As shown in the figure, the acceleration levels imposed on individual ballast particles under train loading can be significantly different depending on the position of the ballast particle with respect to the load position. Two important observations can be made from the data presented in Fig. 10. Firstly, the acceleration levels for the individual particles reduce significantly as the distance of the particle increases from the bottom of the tie. Accordingly, the acceleration levels observed for a particle 300 mm below the bottom of the tie (Fig. 10-d) is significantly lower than particles located 150 mm below the bottom of the tie (see Fig. 10-a and -b). Note that this is already expected since the boundary underneath the ballast layer was assumed to be rigid and non-deformable. Secondly, the particle acceleration can change significantly with lateral position, even at the same depth from the bottom of the tie. This is clearly apparent when two different particles at 150 mm below the bottom of the tie are compared in Fig. 10-a, and -b. Although both these particles are at the same depth, the acceleration time histories for the two particles are quite different from each other. This difference can be attributed to the mechanism of load transfer within a particulate layer. According to previous research (Oda, 1974; Tutumluer, 1995), the load transfer within a granular material is usually along a continuous column of particles. Hence, the acceleration induced on an individual particle is largely dependent on its position with respect to the load transfer column.

Particles between the load transfer columns only provide lateral support, but do not carry much load. Therefore, the vertical accelerations induced in these particles can be significantly lower compared to those lying directly along the load transfer columns. For example, the particle corresponding to the acceleration levels reported in Fig. 10-a lies directly along a load transfer column, therefore

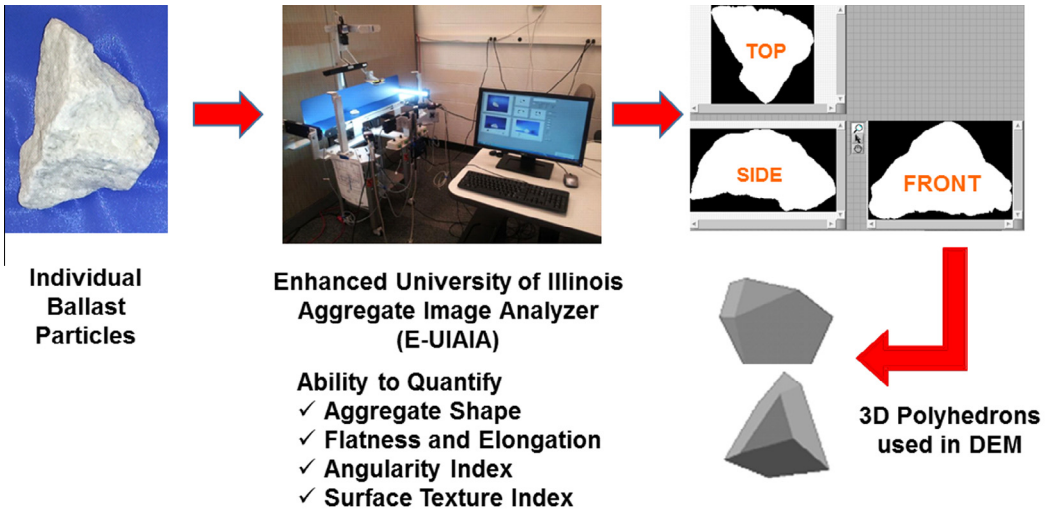

Fig. 8. Half track model generated using Discrete Element Method.

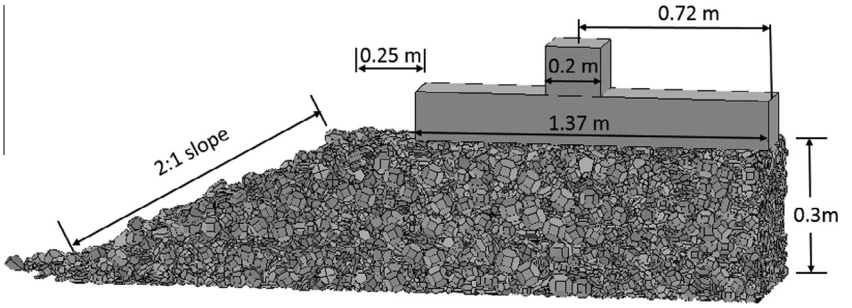

Fig. 9. Comparing the particle acceleration levels at different positions within the ballast layer: (a) 15 cm below bottom of tie: position 1; (b) 15 cm below bottom of tie: position 2; (c) 20 cm below bottom of tie; (d) 30 cm below bottom of tie.

showing distinctive peaks corresponding to each load pulse. However, the particle represented in Fig. 10-b lies adjacent to the load transfer column, resulting in lower peaks corresponding to each load pulse. Similarly, the acceleration values gradually decrease as the distance of a particle from the load transfer column is increased. A similar decrease in particle acceleration values is noticed as the vertical distance from the bottom of the tie is increased. The acceleration values approach zero at a distance of 300 mm from the bottom of the tie since the boundary underneath the ballast layer was assumed to be rigid and non-deformable. Fig. 11 presents a vector plot illustrating the load concentration within the ballast layer right underneath the rail. It can clearly be seen that the magnitude of inter-particle force distribution in vertical direction within the ballast layer is largely dependent on the position of the particle of interest with respect to the load position (rails).

From the above reported results, it is evident that particle acceleration values within a ballast layer can be significantly different depending on the location of the ballast particle with respect to the load position. Using one acceleration value for the entire layer is therefore erroneous, and can be misleading as far as characterizing the dynamic behavior of individual layers is concerned. This highlights a major shortcoming of analysis approaches based on the principles of finite element or finite difference methods that characterize the ballast layer as one continuum, and assign one acceleration value to the entire layer. Note that the graphs presented in Fig. 10 correspond to results from the numerical simulations only. This is because track substructure layer accelerations were not measured under the scope of the current study. Transient deformations of the ballast layer were measured using the MDDs, and the associated layer accelerations have been presented in Fig. 3. An ongoing research study being carried out by the researchers involves track acceleration measurements at different positions within the ballast layer. Results from this study will be included in future publications.

Limitations of the integrated approach in its current form

Although the integrated approach presented in this paper marks a significant improvement over continuum-based approaches, its current implementation has the following limitations:

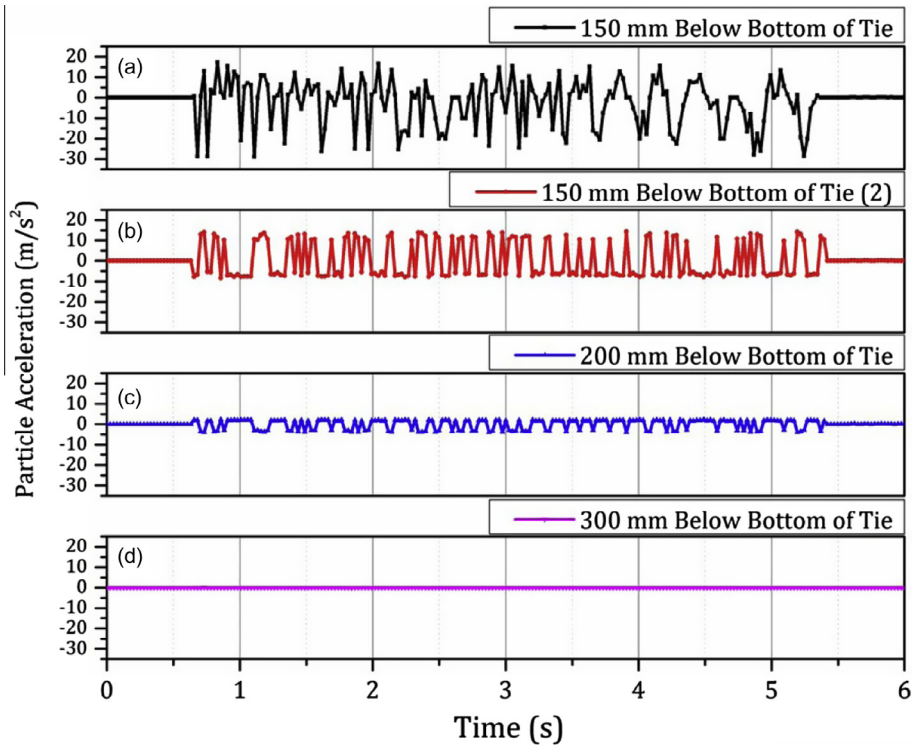

Fig. 10. Comparing the particle acceleration levels at different positions within the ballast layer: (a) 15 cm below bottom of tie: position 1; (b) 15 cm below bottom of tie: position 2; (c) 20 cm below bottom of tie; (d) 30 cm below bottom of tie.

(1) The top LVDT was installed within the concrete crosstie just above the top of the ballast layer. Therefore, nonuniform support conditions underneath the crosstie can lead to different displacement time histories for the crosstie and the ballast layer.
(2) The effects of ballast degradation on the differential movement at track transitions have not been considered in the analyses.
(3) The current implementation of the dynamic track model reported in this paper does not account for missing and/or disintegrated ties. Consideration of the missing and/or disintegrated ties can lead to a different load time history on top of the ballast layer, thus changing the results reported in this paper.
(4) The boundary immediately underneath the ballast layer has been modeled as non-deformable within the BLOKS3D DEM program. This may potentially lead to different damping characteristics near the bottom boundary, thus affecting the predicted acceleration values.
(5) Particle acceleration values reported in this paper have been obtained from only one simulation run. Repeated simulations using the BLOKS3D program

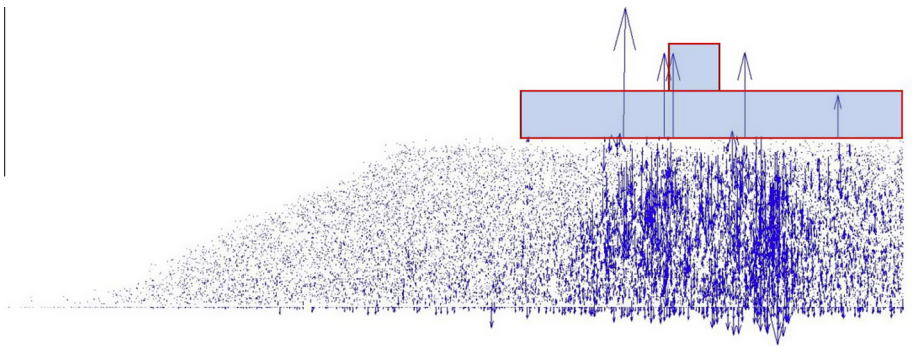

Fig. 11. Vector plot showing load concentration underneath the rail as predicted from the discrete element simulation.

are currently being performed to account for different initial conditions during the ballast layer compaction.

(6) Particle accelerations reported in this paper need to be verified through additional instrumentation comprising the placement of accelerometers at different positions within the ballast layer.

Summary and conclusions

This paper presented an integrated approach to dynamic analysis of railway track transitions through combined application of field instrumentation along with analytical and numerical modeling. Several problematic bridge approaches were instrumented to monitor the track response under loading Amtrak's North East Corridor (NEC) in south of Philadelphia near Chester, Pennsylvania. Track deformation and load data from the instrumented bridge approaches were then used to calibrate a fully-coupled 3-dimensional track dynamic model. Loading profiles generated from this model were used as input for a numerical simulation program based on the Discrete Element Method (DEM) to predict individual particle accelerations within the ballast layer. Analysis results have clearly indicated that particle acceleration values within a ballast layer can be significantly different depending on the location of the ballast particle with respect to the load position. Accordingly, characterizing the ballast layer as a continuum and assigning one acceleration value to the entire layer may lead to erroneous predictions of dynamic track behavior. The ballast layer is a particulate medium and the particle to particle nature of wheel load transfer within the ballast layer needs to be carefully considered in dynamic track vehicle interaction modeling.

Acknowledgements

The authors would like to acknowledge the efforts of Mr. Yin Gao, graduate student at the Pennsylvania State University, and Mr. Huseyin Boler and Ms. Wenting Hou, graduate students at the University of Illinois for their help with the analytical modeling and data analyses efforts. The help of Mike Tomas, Marty Perkins, and Carl Walker of AMTRAK, Hasan Kazmee, Mike Wnek, and James Pforr of University of Illinois during the field instrumentation efforts is greatly appreciated. Field instrumentation data reported in this paper were collected under the scope of an ongoing research study at the University of Illinois, titled "Mitigation of Differential Movement at Railway Transitions for US High Speed Passenger Rail and Joint Passenger/Freight Corridors." The authors acknowledge the contributions of Dr. James P. Hyslp and Dr. Timothy D. Stark for their assistance in the above mentioned research project.

References

Briaud JL, James RW, Hoffman SB. Settlement of bridge approaches (the bump at the end of the bridge). Washington, D.C.: Transportation Research Board; 1997.

Briaud JL, Nicks NE, Smith BJ. The bump at the end of the railway bridge: final report. Texas A&M University; 2006.

Chang CS, Adegoke CW, Selig ET. The GEOTRACK model for railroad track performance. J Geotech Eng Div ASCE 1980;106(GT11):1201–18.

DeBeer M, Horak E, Visser A. The multidepth deflectometer (MDD) system for determining the effective elastic moduli of pavement layers. Nondestr Test Pavement Backcalculation Moduli ASTM STP 1989;1026:70–89.

Ghaboussi J, Barbosa R. Three dimensional discrete element method for granular materials. Int J Numer Anal Methods Geomech 1990;14(7):451–72.

Gräbe PJ, Clayton C. Designing railway formations for the future. Civil Eng 2005;13(5).

Gräbe PJ, Shaw FJ. Design life prediction of a heavy haul track foundation. Proc Inst Mech Eng F 2010;224(5):337–44.

Huang H, Brennecke B. Track stiffness transition zone studied with three-dimensional sandwich track model. Transp Res Rec 2013;2374(1):136–42.

Huang H, Tutumluer E. Discrete element modeling for fouled railroad ballast. Constr Build Mater 2011;25(8):3306–12.

Huang H, Shen S, Tutumluer E. Sandwich model to evaluate railroad asphalt trackbed performance under moving loads. Transp Res Rec 2009;2117:57–65.

Huang H, Shen S, Tutumluer E. Moving load on track with Asphalt trackbed. Veh Syst Dyn 2010;48(6):737–49.

Huang H, Gao Y, Stoffels S. A fully coupled 3D train–track–soil model for high-speed model. Transp Res Rec 2014:1–13.

Hyslip JP, Li D, McDaniel CR. Railway bridge transition case study. In: Tutumluer E, Al-Qadi I, editors. Proceedings of eighth international conference on bearing capacity of roads, railways and airfields, Champaign, Illinois 2009;No. II. Champaign, Illinois: University of Illinois at Urbana-Champaign; 2009. p. 1341–8.

Mishra D, Tutumluer E, Stark TD, Hyslip JP, Chrismer SM, Tomas M. Investigation of differential movement at Railroad Bridge approaches through geotechnical instrumentation. J Zhejiang Univ Sci A 2012;13(11):814–24.

Nezami EG, Hashash YMA, Zhao D, Ghaboussi J. Shortest link method for contact detection in discrete element method. Int J Numeri Anal Methods Geomech 2006;30(8):783–801.

Nicks JE. The bump at the end of the Railway Bridge [Ph.D. thesis]. Texas A&M University; 2009.

Oda M. A mechanical and statistical model of granular material. Soils Found 1974;14(1):13–27.

Plotkin D, Davis DD. Bridge approaches and track stiffness. Publication final report: DOT/FRA/ORD-08/01. U.S. Department of Transportation: Federal Railroad Administration; Feb. 2008. p. 1–45.

Priest JA, Powrie W, Yang L, Gräbe PJ, Clayton CRI. Measurements of transient ground movements below a ballasted railway line. Géotechnique 2010;60(9):667–77.

Rao C, Tutumluer E, Stefanski JA. Coarse aggregate shape and size properties using a new image analyzer. J Test Eval 2001;29(5):461–71.

Rao C, Tutumluer E, Kim IT. Quantification of coarse aggregate angularity based on image analysis. Transp Res Rec 2002;1787:117–24.

Rao C, Pan T, Tutumluer E. Determination of coarse aggregate surface texture using image analysis. Presented at the proceedings of the pavement mechanics symposium at the 16th ASCE engineering mechanics division conference (EM2003). Seattle, Washington; 2003.

Read D, Li D. Design of track transitions. Publication research result digest 79. Transit cooperative research program, Federal Transit Administration; Oct. 2006. p. 1–38.

Sasaoka CD, Davis DD, Koch K, Reiff RP, GeMeiner W. Implementing track transition solutions. Technol Digest 2005;TD-05-001:1–4.

Scullion T, Briggs RC, Lytton RL. Using the multidepth deflectometer to verify modulus backcalculation procedures. Presented at the nondestructive testing of pavements and backcalculation of moduli. ASTM STP; 1989. 1026.

Stark TD, Olson SM, Long JH. Differential movement at the embankment/structure interface – mitigation and rehabilitation. Publication Project-ECT IAB-H1 FY 93. Illinois Transportation Research Center; 1995.

Stewart HE, Selig ET. Predicted and measured resilient response of track. J Geotech Eng Div ASCE 1982a;108(11):1423–42.

Stewart HE, Selig ET. Predictions of track settlement under traffic loading. Presented at the second international heavy haul railway conference; 1982.

Tutumluer E. Predicting behavior of flexible pavements with granular bases. Atlanta, Georgia: Georgia Institute of Technology; 1995.

Tutumluer E, Huang H, Hashash Y, Ghaboussi J. Aggregate shape effects on ballast tamping and railroad track stability. Presented at the AREMA 2006 annual conference. Louisville, Kentucky; 2006.

Tutumluer E, Huang H, Hashash Y, Ghaboussi J. Discrete element modeling of railroad ballast settlement. Presented at the AREMA 2007 annual conference; 2007.

Tutumluer E, Qian Y, Hashash Y, Ghaboussi J, Davis DD. Field validated discrete element model for railroad ballast. Presented at the AREMA 2007 annual conference; 2011.

Vorster DJ, Gräbe PJ. The Effect of axle load on track and foundation resilient deformation under heavy haul conditions. Presented at the 10th international heavy haul association conference, New Delhi, India; 2013.

White D, Sritharan S, Suleiman M, Mekkawy M, Chetlur S. Identification of the best practices for design, construction, and repair of bridge approaches. Center for Transportation Research and Education, Iowa State University; 2005.

Zaman M, Gopalasingam A, Laguros JG. Consolidation settlement of bridge approach foundation. J Geotech Eng 1991;117(2):219–40.